Quantum weak chaos in a degenerate system

V. Ya. Demikhovskii and D. I. Kamenev
Nizhny Novgorod State University, Nizhny Novgorod 603600, Russia

G. A. Luna-Acosta
Instituto de Fisica, Universidad Autonoma de Puebla, Apartado Postal J-48, Puebla 72570, Mexico
(Received 26 February 1998)

Quantum weak chaos is studied in a perturbed degenerate system: a charged particle interacting with a monochromatic wave in a transverse magnetic field. The evolution operator for an arbitrary number of periods of the external field is built and its structure is explored in terms of the quasienergy eigenstates under resonance conditions (when the wave frequency equals the cyclotron frequency) in the regime of weak classical chaos. The new phenomenon of diffusion via the quantum separatrices and the influence of chaos on diffusion are investigated and, in the quasiclassical limit, compared with its classical dynamics. We determine the crossover from purely quantum diffusion to a diffusion that is the quantum manifestation of classical diffusion along the stochastic web. This crossover results from the nonmonotonic dependence of the characteristic localization length of the quasienergy states on the wave amplitude. The width of the quantum separatrices was computed and compared with the width of the classical stochastic web. We give the physical parameters that can be realized experimentally to show the manifestation of quantum chaos in a nonlinear acoustic resonance.
[S1063-651X(98)10412-9]

PACS number(s): 05.45.−a, 03.65.−w

I. INTRODUCTION

The problem of quantum chaos in intrinsically degenerate systems possesses a number of interesting properties. The Kol'mogorov-Arnol'd-Moser (KAM) theorem in these systems is not applicable [1] and in certain models an arbitrary small perturbation is sufficient to induce an infinite stochastic web in phase space. The character of the web is determined by the type of perturbation. When the system is perturbed by a monochromatic wave, the web width exponentially decreases with increasing action I and the motion is practically localized [2]. If the perturbation has the form of periodic δ impulses, the web width is constant and the particle, traveling along the web, can diffuse to infinity [2] (see also Refs. [3,4]). In both cases the web in (p,x) phase space has a crystalline or quasicrystalline structure. The chaotic motion in these systems has been termed weak chaos since chaos occupies only a small portion of phase space (see e.g., Ref. [2]). In contrast, in strong (or global) chaos, the web structure disappears and most of the phase space is filled with chaotic orbits. The peculiar resonance structure and the appearance of an infinite stochastic web make degenerate systems very attractive objects in which to study quantum manifestations of chaos.

The problem of weak and strong chaos has been mainly explored within the context of the kicked harmonic oscillator [5,6]. It has been shown that the time of the classical description of quantum averages is considerably longer for weak than for strong chaos. The role of the symmetry of the quasienergy (QE) functions was also analyzed in Ref. [5]. It was found that under certain conditions, quantum diffusion within the stochastic web was truncated by quantum interference effects [6], similar to the case of strong chaos in the kicked rotor [7]. The problem of quantum chaos on the stochastic web has also been studied intensively in recent years within the framework of the generalized kicked Harper model [8,9]. Another simple and yet important (especially to solid state physics) example of a degenerate system is that of a charged particle moving in a uniform magnetic field and interacting with a monochromatic wave, propagating perpendicularly to the magnetic field direction under the condition of cyclotron resonance. This two-dimensional problem is tantamount to the one-dimensional harmonic oscillator in a wave field [3,10]. In our previous work [11] we studied this system quantum mechanically, focusing on the resonance approximation, which appears as the first-order perturbation for the Floquet Hamiltonian. In the quasiclassical limit the dynamics in the resonance approximation is globally regular in phase space. The structure of the Floquet spectrum and the QE eigenfunctions for the exact and near-resonance cases were obtained and related to the classical phase space structure. The evolution of various representative initial states was investigated and the close connection between classical and quantum dynamics at the cyclotron resonance was demonstrated. In Ref. [12] it was shown that the boundaries of the quantum cells act as dynamical barriers to the probability flow. In the quasiclassical limit the dynamical barriers were found to correspond to the separatrices in classical phase space and tunneling through the ''quantum separatrices'' was explored numerically.

In the present work we study the dynamical effects of chaos on the above-mentioned system under the condition of cyclotron resonance $\omega=\omega_c$ (ω and ω_c are the wave and cyclotron frequencies, respectively). This model seems to be more closely related to experimental realizations in solid state physics than the kicked system. The evolution operator for an arbitrary number of periods of the external field is built and its structure is explored in terms of the QE eigenstates under the conditions of weak chaos. The structure of the evolution operator matrix is more complex than the more

typical bandlike matrix structure. Thus the usual diagnostics of quantum chaos predicted by band random matrix theory [13,14] do not work in the case of weak chaos because only a small number of QE eigenstates are affected by the perturbation. A new phenomenon of diffusion over the quantum separatrices and the effect of weak chaos on the diffusion are investigated here and compared in the quasiclassical limit with the dynamics in classical phase space. The crossover from purely quantum diffusion to a diffusion that in the quasiclassical limit corresponds to classical diffusion within the stochastic web is determined. The width of the quantum separatrices is computed and compared with the width of the classical stochastic web.

The paper is organized as follows. In Sec. II the basic model is introduced. Also in Sec. II the structures of the nonstationary Schrödinger equation and the evolution operator in $\hat{H}_0$ representation are discussed. In Sec. III the properties of the QE eigenstates are described. The phenomenon of diffusion via the quantum separatrices and the influence of chaos on the diffusion are investigated numerically in Sec. IV. In Sec.V we draw our conclusions.

II. EVOLUTION OPERATOR

The Hamiltonian of a charged particle in a magnetic field interacting with a monochromatic wave reads

$$\hat{H}=\frac{\left(\hat{\mathbf{p}}+\frac{e}{c}\mathbf{A}\right)^2}{2m}+v_0\cos(kx-\omega t)=\hat{H}_0+\hat{V}(x,t), \quad (1)$$

where m and e are, respectively, the mass and charge of the particle, $\hat{\mathbf{p}}$ is the momentum, k is the wave vector, ω is the wave frequency, and v_0 is the amplitude of the perturbation. We choose the gauge of $\mathbf{A}$ in the form $\mathbf{A}=(0,Hx,0)$ so as to have the magnetic field $\mathbf{H}$ along the z direction and to have the momentum p_y as an integral of motion. The Hamiltonian is equivalent to a one-dimensional simple harmonic oscillator perturbed by a monochromatic wave field. Hence the problem is to determine the dependence of the wave function on only two variables x and t.

It is convenient to expand the state vector in the harmonic oscillator basis

$$\psi(x,t)=\sum_n C_n(t)\psi_n(x)\exp(-iE_nt/\hbar), \quad (2)$$

where $\psi_n(x)$ is the nth eigenfunction of the simple harmonic oscillator Hamiltonian $\hat{H}_0$ and $E_n=\hbar\omega_c(n+1/2)$ is the energy of the nth Landau level. Using Eq. (2), the nonstationary Schrödinger equation

$$i\hbar\frac{\partial\psi(x,t)}{\partial t}=\hat{H}\psi(x,t) \quad (3)$$

yields a set of differential-difference equations for the coefficients $C_n(t)$,

$$i\hbar\dot{C}_n=v_0\sum_m\left[V^{(1)}_{n,n+m}\sin(\omega t)+V^{(2)}_{n,n+m}\cos(\omega t)\right]C_{n+m}e^{-im\omega_c t}. \quad (4)$$

The matrix elements $V^{(1)}_{n,n+m}$ ($V^{(2)}_{n,n+m}$) describe the transitions between the levels of opposite (equal) parity and can be expressed via the Laguerre polinomials as [11]

$$V^{(1)}_{n,n+2m+1}=\frac{(-1)^m h^m e^{-h/4}}{2^{m+1}\sqrt{(n+1)\cdots(n+2m+1)}}L_n^{2m+1}\left(\frac{h}{2}\right), \quad (5a)$$

$$V^{(2)}_{n,n+2m}=\frac{(-1)^m h^m e^{-h/4}}{2^{m+1}\sqrt{(n+1)\cdots(n+2m)}}L_n^{2m}\left(\frac{h}{2}\right), \quad (5b)$$

where $h=(ka)^2$ plays the role of an effective (dimensionless) Planck constant and $a=\sqrt{\hbar c/e\mathrm{H}}$ is the magnetic length. For $n\gg 1\gg h$ the matrix elements can be approximated in terms of the Bessel functions J_m of order m by [15]

$$V^{(1)}_{n,n+2m+1}=\frac{1}{2}\frac{(-1)^m n^{m+1/2}e^{-h/4}}{\sqrt{(n+1)\cdots(n+2m+1)}}J_{2m+1}(\sqrt{2nh}), \quad (6a)$$

$$V^{(2)}_{n,n+2m}=\frac{1}{2}\frac{(-1)^m n^m e^{-h/4}}{\sqrt{(n+1)\cdots(n+2m)}}J_{2m}(\sqrt{2nh}). \quad (6b)$$

Since the perturbation is periodic in time, Floquet theory can be used to describe the time evolution of the system in terms of the QE spectra ε_q and the QE eigenfunctions $\psi_q(x,t)$. The QE states are the eigenstates of the evolution operator $\hat{U}$ for one period of oscillation of the external field $T=2\pi/\omega$,

$$\hat{U}(T)\psi_q(x,t)=\exp\left(-\frac{i\varepsilon_q T}{\hbar}\right)\psi_q(x,t),$$

which can be defined by (see, for example, Ref. [16], p. 385)

$$\psi_q(x,t)=\exp\left(-\frac{i\varepsilon_q t}{\hbar}\right)\sum_n C_n^q(t)\psi_n(x)=\exp\left(-\frac{i\varepsilon_q t}{\hbar}\right)u_q(x,t), \quad (7)$$

where the functions $C_n^q(t)$ and $u_q(x,t)$ are periodic in time, $u_q(x,t+T)=u_q(x,t)$.

The coefficients $C_n^q(t)$ are the eigenvectors of the operator $\hat{U}$ in the representation of the Hamiltonian $\hat{H}_0$ and can be found by diagonalizing the corresponding matrix $U_{n,m}$. The following procedure is one way to obtain the matrix elements [17]. Let the evolution operator $\hat{U}$ act on the initial state $C_n^{(n_0)}(0)=\delta_{n,n_0}$,

$$U_{m,n}(T)C_n^{(n_0)}(0)=U_{m,n_0}(T)=C_m^{(n_0)}(T). \quad (8)$$

The coefficients $C_m^{(n_0)}(T)$ can be computed numerically by integration of Eq. (4). They form a column in the matrix $U_{m,n_0}(T)$. Repetition of this process for initial states, orthogonal to the previous one, $C_n^{n'}(0)=\delta_{n,n'}$, $n'\neq n_0$, fills the matrix $U_{m,n_0}(T)$. Diagonalization of the matrix $U_{m,n}(T)$ yields the eigenvalues ε_q and the eigenvectors C_n^q. The number of the Landau levels N in Eqs. (2) and (4) included in our computations is equal to the size of the evolution operator matrix $U_{m,n}(T)$ and hence to the number of its QE eigenstates.

Once the eigenvalues ε_q and the eigenvectors C_n^q are obtained, we may write the evolution operator for one period $U_{m,n}(T)$ in the form [16]

$$U_{n,n'}(T)=\sum_q C_n^q C_{n'}^{q*}\exp(-i\varepsilon_q T/\hbar). \tag{9}$$

By raising $U_{n,n'}(T)$ to degree M and using the orthogonality of the eigenvectors C_n^q, one can obtain the evolution operator that propagates the system toward M periods $U_{n,n'}(MT)$ by

$$U_{n,n'}(MT)=\sum_q C_n^q C_{n'}^{q*}\exp\left(-i\frac{\varepsilon_q MT}{\hbar}\right). \tag{10}$$

Given $U_{n,n'}(MT)$, the evolution of any initial state $C_n(0)$ can be computed by using

$$C_n(MT)=\sum_{n'} U_{n,n'}(MT)C_{n'}(0). \tag{11}$$

The expressions (10) and (11) are much more practical for calculations than the integration of the set of differential equations (4), especially in the limit $t\to\infty$, because they allow us to obtain the state of the system at any time t by a simple summation. There are only two dimensionless parameters determining the dynamics of the system, namely, the dimensionless amplitude of the perturbations $V_0=v_0/\hbar\omega$ and the effective Planck constant h in the arguments of the matrix elements (5a) and (5b). This is easy to see if we write Eq. (4) in dimensionless form by introducing the dimensionless time $\tau=t\omega V_0$. In this form, the phases of the oscillating terms are given by $-m\tau/V_0$. Thus the larger the amplitude of the wave V_0, the smaller the frequency of the oscillations and the larger the number of effective terms that participate in the dynamics. Consequently, the parameter V_0 determines the number of effective terms on the right-hand side of Eq. (4), which can be roughly estimated as $m\geqslant V_0$. The same estimation yields the bandwidth of the evolution operator matrix (8) or (9). If $V_0\ll 1$ the resonant terms with $m=\pm 1$ dominate the dynamics; they become independent of time since they are being multiplied by $\sin(\omega t)$ or $\cos(\omega t)$. The other terms oscillate fast and can be averaged out. Consideration of only these time-independent coefficients constitutes what we call the resonance approximation. As was shown in Refs. [11,12], the quantum resonance approximation in the quasiclassical limit in general corresponds to the classical resonance approximation (see, e.g., Ref. [18]). It is necessary to point out that when $V_0\geqslant 1$, the matrix elements $V_{n,n+m}\sim J_m(\sqrt{2nh})$ decrease quickly with m in the region $m>\sqrt{2nh}$ and this inequality can be treated as an additional restriction on the bandwidth of the evolution operator matrix.

As V_0 increases, the number of effective terms increases too. This number was numerically determined by requiring relatively small changes in the QE spectrum and in the QE eigenfunctions after including an additional term to the sum (4). The fluctuations did not exceed the accuracy of the Runge-Kutta method used for integration of Eq. (4). The numerically determined number of effective terms was found to be of the order of V_0, in agreement with the speculations presented above. The Runge-Kutta procedure was controlled by the normalization condition $\Sigma_n|C_n|^2=1$; the fluctuations of this value were smaller than 10^{-4}.

III. SEPARATRIX QUASIENERGY EIGENSTATES

In this section we discuss the structure of the QE states that determine the dynamics via Eqs. (10) and (11). We first consider the resonance approximation, which will be the starting point for the investigation of quantum chaotic effects in next-order approximations [11,12]. The equation for the QE eigenstates in the resonance approximation can be obtained by putting the QE eigenfunction in the form (7) into Eq. (4) and keeping only time-independent (resonance) terms. Thus the set of differential-difference equations (4) is transformed into the set of algebraic equations

$$E_q C_n^q=V_0(V_{n,n+1}C_{n+1}^q+V_{n,n-1}C_{n-1}^q), \tag{12}$$

where $E_q=\varepsilon_q/\hbar\omega$ is the dimensionless quasienergy. This is an eigenvalue problem for the Floquet Hamiltonian [12]. Equation (12) is similar to the Harper equation in the symmetric gauge of the vector potential $\mathbf{A}$ with periodic off-diagonal modulation of the matrix elements [19]. In our case the off-diagonal modulation is nonperiodic. The dependence of the matrix elements $V_{n,n+1}$ on the Landau number n is shown in the upper part of Fig. 1. Due to oscillations of $V_{n,n+1}$ and $V_{n,n-1}$ with n, the Floquet Hamiltonian matrix for determining the QE eigenstates (12) has a cell structure; the boundaries of the cell are given by the zeros of the Bessel function [cf. Eq. (6a)]. One can easily show that at small values of E_q ($V_0\ll 1$) the Floquet Hamiltonian matrix (12) can be obtained from the Floquet matrix (9). Moreover, as will be shown below, the cell structure is maintained even for very large values of V_0 ($V_0\sim 10$); an extremely strong perturbation amplitude is required to destroy the cells entirely. The regions where the matrix elements $V_{n,n+1}$ are small [one such region is marked with the rectangle in the plot $V_{n,n+1}(n)$ in Fig. 1] can be referred to as quantum separatrices because in the quasiclassical limit their positions in action I correspond to the positions of the classical separatrices in phase space [11,12]. These are given by the zeros of the Bessel function of order 1.

The structure of the QE eigenfunctions can be understood by characterizing each one by its center $\overline{n_q}=\Sigma_n n|C_n^q|^2$ and its dispersion $\sigma_q=[\Sigma_n(n-\overline{n_q})^2|C_n^q|^2]^{1/2}$. The plot of $\overline{n_q}$ versus σ_q in the resonance approximation is shown on the left-hand side of Fig. 2(a); the figures on the right-hand side are the Poincaré surfaces of sections for the classical system with the same parameters. Each point in the plot $\overline{n_q}(\sigma_q)$

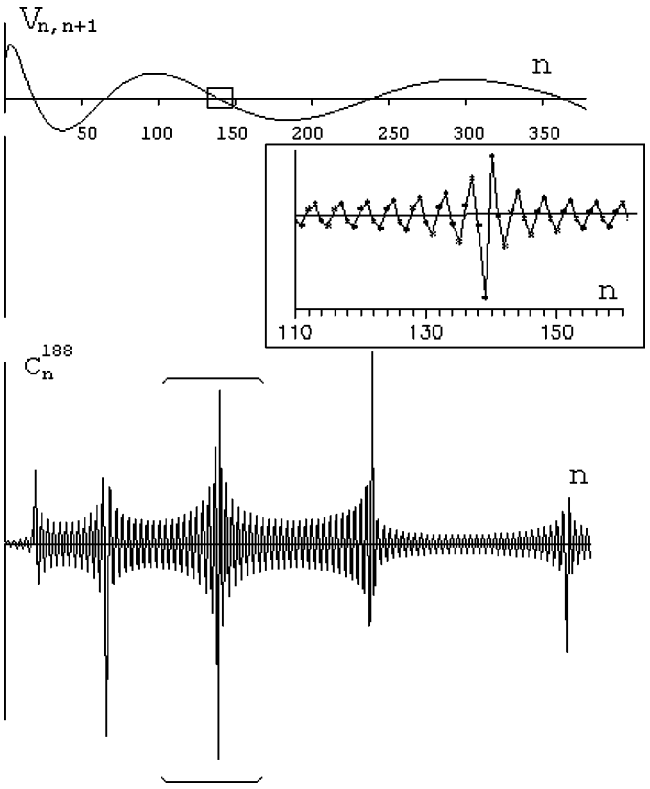

FIG. 1. Matrix elements $V_{n,n+1}$ in dimensionless units versus the Landau number n (upper part) and the most delocalized QE eigenfunction in the resonance approximation (lower part). The inset amplifies a small portion of the QE eigenfunction, marked with brackets. Here $h=0.37$ and $V_0=0.002$.

corresponds to two QE eigenstates (E_q and $-E_q$) due to the symmetry of Eq. (12) under the transformation

$$E_q \rightarrow -E_q, \quad C_n^q \rightarrow (-1)^n C_n^q, \tag{13}$$

corresponding to the transformation $x \rightarrow -x$ in Eq. (7). It is seen that almost all the QE eigenfunctions are divided into groups with practically the same $\overline{n}_q$ and different σ_q. Each group of states belongs to only one resonant cell because the $\overline{n}_q$ for each QE eigenfunction is situated in the center of the cell and $\overline{n}_q \pm \sigma_q$ does not exceed the size of the corresponding cell [the boundaries of the cells in Fig. 2(a) are marked with arrows]. It was shown in Ref. [12] that the Husimi function [20] of a QE state with quasienergy $E_q>0$ is localized in the upper part ($x>0$) of the phase space and the Husimi function of a state with $-E_q$ is situated in the lower part ($x<0$). Thus each row on the left-hand side of Fig. 2(a) corresponds to the two symmetrical classical resonance cells shown on the right-hand side of Fig. 2(a): The first row is associated with two classical cells near the point ($x=0, p=0$), the second row with the next symmetrical classical cells, and so on. The number of the QE eigenfunctions in an individual cell equals approximately the number of the Landau states in this cell.

Besides the localized eigenfunctions [arranged in rows in Fig. 2(a)], there are a small number (3–4 %) of delocalized states that cannot be assigned to any particular cell; they are represented by the scattered points. These QE eigenfunctions have large dispersions, with σ_q exceeding the size of one cell. Hereinafter we shall characterize the ''localization length'' of the QE functions by σ_q. It was found numerically that the most localized eigenfunctions correspond to the largest QE eigenvalues (in absolute value), while the most delocalized states correspond to one of the smallest eigenvalues. Calculations with other values of the effective Planck constant h have shown that the number of delocalized QE eigenstates increases with increasing h, which indicates that, as will be shown below, these states are of a pure quantum nature with no classical analogs. A representative delocalized eigenfunction, the widest one, marked in Fig. 2(a) with an arrow, is shown in the lower part of Fig. 1 and its Husimi function is plotted in Fig. 3. Note that the eigenfunction and the Husimi function have their maxima in the regions of the classical separatrices [cf. Fig. 2(a)]. Thus the delocalized states can be identified as ''separatrix eigenstates.'' The Husimi function in Fig. 3 is symmetrical with respect to $p \rightarrow -p$ but not symmetrical under the transformation $x \rightarrow -x$, which turns the Husimi function corresponding to the eigenvalue E_q into the one corresponding to $-E_q$ [see Eq. (13)]. The high peaks in Fig. 3 near the separatrix line $x=0$ result from the slowing of the motion of the classical particle, which in turn increases the probability of finding the particle in this region. The existence of fully delocalized eigenstates of the matrix $U_{n,m}(T)$ is a very interesting, nontrivial feature. Initially (time $M=0$), the QE functions, due to their completeness, yield a Kroenecker delta $\delta_{n,n'}$ in Eq. (10). If n and n' belong to different cells, then only a small number of the delocalized QE functions provide the cancellation of terms in Eq. (10). The condition of completenes (10) (at $M=0$) serves as a good check for our numerical calculations. At short times ($M \sim 1$) in the resonance approximation, where $V_0 \ll 1$, one may take into consideration only the elements along the first off diagonal of the matrix $U_{n,m}$, which are of the order of E_q; the elements in the second off diagonal will be of the order of $(E_q)^2$ and so on. Let us estimate the width Δn_i of the maxima of the separatrix eigenfunctions, where the index i labels the separatrix number. To this end we approximate the matrix element $V_{n,n+1}$ near the separatrices by the linear function (see the upper part of Fig. 1) $V_{n,n+1}=V_{n_0,n_0+1}+\alpha(n-n_0)$. Here n_0 is the Landau state number where the value of the matrix element $V_{n,n+1}$ is minimum and $\alpha=\partial V_{n_0,n_0+1}/\partial n$. This approximation is valid when the separatix region Δn_i is smaller than the total number of the Landau states in the ith cell n_i, $\Delta n_i \ll n_i$. Under this condition, Eq. (12) takes the form

$$\frac{E_q}{V_0} C_n^q = [V_{n_0,n_0+1} + \alpha(n-n_0)] C_{n+1}^q + [V_{n_0,n_0+1} + \alpha(n-n_0-1)] C_{n-1}^q. \tag{14}$$

For the separatrix states, the ratio E_q/V_0 is of the order of 10^{-3} and one can omit the left-hand side of Eq. (14); the minimal matrix element V_{n_0,n_0+1} near the separatrix is also small and may be neglected as well. Under these assumptions, Eq. (14) gives the relation between the coefficients C_n^q,

$$C_{n_0+m}^q = \frac{m}{m+1} \frac{m-2}{m-1} \cdots \frac{1}{2} C_{n_0-1}^q. \tag{15}$$

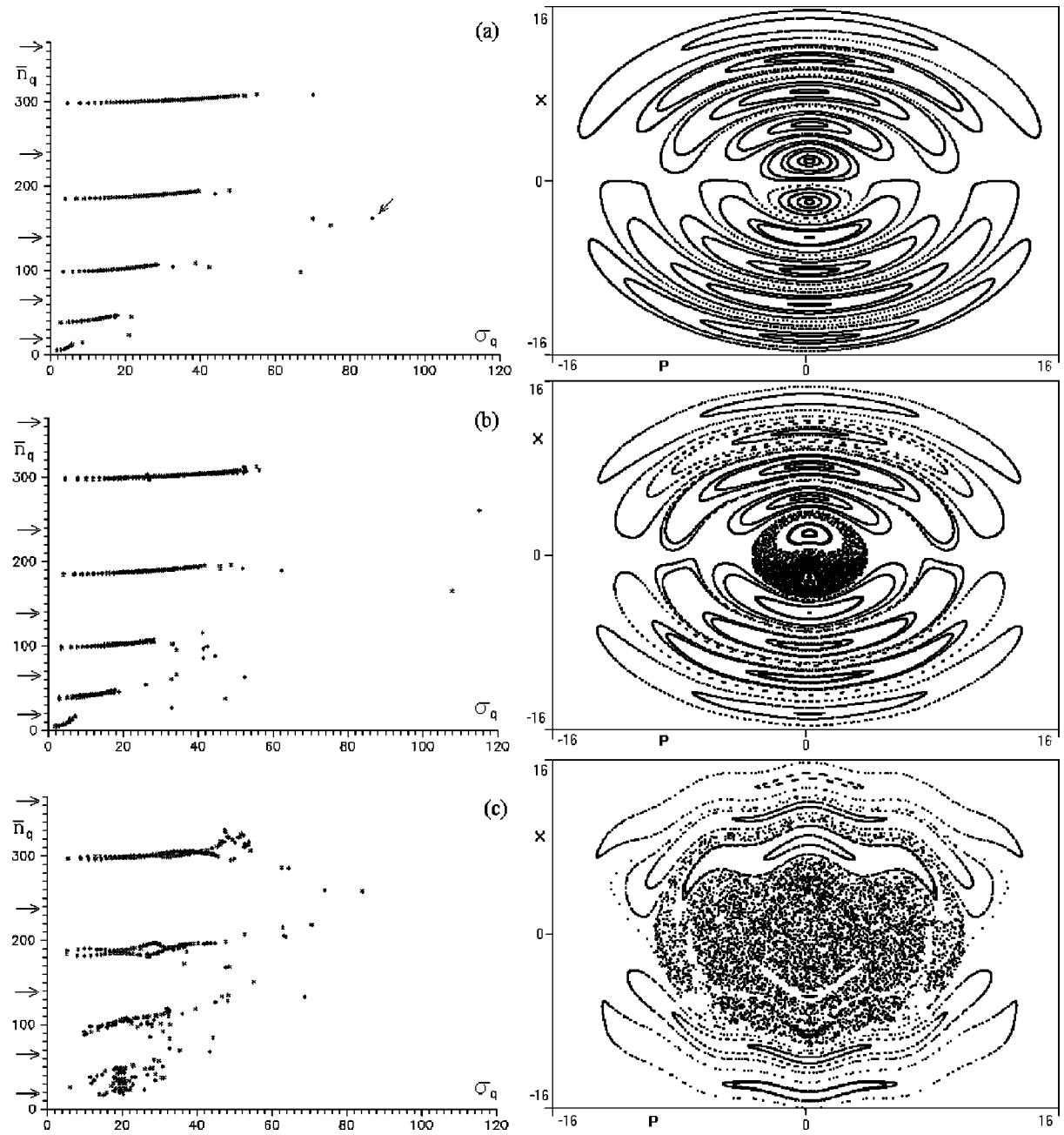

FIG. 2. Plot of the dispersions σ_q versus $\overline{n_q}$ for the QE eigenfunctions with $q=1,2,\ldots,N$ for $h=0.37$, $N=381$, and different values of V_0: (a) $V_0=0.002$, (b) $V_0=6$, and (c) $V_0=13$ (left-hand side) and classical phase space for the same parameters (right-hand side).

Here $C^q_{n_0-1}$ is the magnitude of the QE eigenfunction in the maximum and m (here odd) is the distance from the maximum (see the inset in Fig. 1). The reduced equation (15) is independent of the parameters and cell number; as a consequence, the separatrix width Δn_i should be the same for all cells. This was confirmed by our numerical calculations discussed below. In the quasiclassical limit, when $h\to 0$ and $n_i\to\infty$, the relative width of the quantum separatrix $\Delta n_i/n_i$ tends to zero, consistent with the classical dynamics.

To conclude our discussion on the structure of the QE eigenstates in the resonance approximation it is necessary to point out that the numerical results obtained by using two different approaches, the Floquet Hamiltonian formalism [16] in Eq. (12) and the Floquet formalism at $V_0\to 0$ described in Sec. II, lead to the same results with very high accuracy. The latter method is nonperturbative and allows us to obtain the solutions at any (not necessarily small) amplitude V_0. In the following discussion this approach will be used to investigate quantum chaos in our system.

In order to incorporate chaos one must increase the perturbation amplitude. The structure of the QE eigenfunctions in the presence of weak chaos is shown in Figs. 2(b) and 2(c). Note the qualitative difference from the results obtained for the resonance approximation [Fig. 2(a)]. Increasing the perturbation amplitude to the value $V_0=6$ [Fig. 2(b)] gives rise to a change in the separatrix eigenstates: Their dispersions σ_q decrease on the average. In contrast, localized eigenfunctions (arranged in rows) are slightly affected by the perturbation, resulting in a small splitting of the rows. This is in close agreement with the classical behavior, namely, the

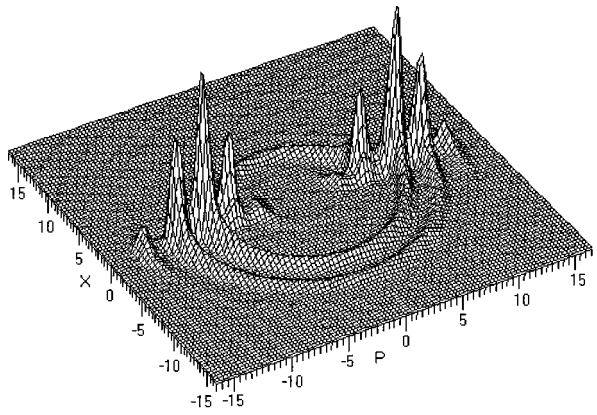

FIG. 3. Husimi function corresponding to the QE eigenstate plotted in Fig. 1.

region around the classical separatrix is first and most affected by an increase of V_0.

A further increase of V_0 to the value $V_0=13$ [Fig. 2(c)] leads to an increase in the number of delocalized states and, on average, the localization length grows again. The most drastic effect of chaos on the quasienergy eigenfunctions was observed in the region of Hilbert space corresponding to completely chaotic motion in classical phase space [the first two cells on the right-hand side of Fig. 2(c)]. The chaos of the corresponding QE eigenfunctions is manifested in the apparent random character of the dependence $\overline{n}_q(\sigma_q)$; each QE eigenfunction spans both cells so that they cannot be assigned to any particular one. Furthermore, our numerical experiments show that the dependence of C_n^q on the Landau number n in the chaotic area is also very irregular. Note that, as in the classical case, perturbation affects the various cells differently: Cells with small values of Landau numbers n appear to be more affected than those with larger n.

In Figs. 2(b) and 2(c) there are no points corresponding to two eigenfunctions as there are in Fig. 2(a) because of the substantial influence of the nonresonant terms on all the QE eigenstates. Recall that in the resonance approximation the system has the symmetry defined by Eq. (13). Weak chaos lifts this symmetry and splits the rows on the left-hand sides of Figs. 2(b) and 2(c). The third and fifth rows correspond to mixed phase space dynamics, shown on the right-hand sides of Figs. 2(b) and 2(c).

IV. QUANTUM DIFFUSION VIA THE SEPARATRICES

The quantum dynamical manifestations of weak chaos are studied in this section by means of the nonperturbative technique based on the Floquet formalism discussed in Sec. II. In the regime of weak chaos only a small portion of phase space is chaotic. Correspondingly, in the quantum model, only a small number of the eigenstates are affected (see Sec. III). However, we expect to detect the influence of weak chaos on the dynamics if we consider the diffusion along the separatrices. This intuition is based on the fact that the diffusion via the separatrices is governed by the separatrix QE eigenstates, which are the ones mainly affected by the perturbation. In order to check this, let us consider the evolution of an initial state $C_n^{n_0}(0)=\delta_{n,n_0}$, which is described by [see Eqs. (10) and (11)]

$$C_n^{n_0}(M)=\sum_q C_n^q C_{n_0}^{q*}\exp(-iE_qM), \tag{16}$$

where time is measured in the number of external field periods M. The value of the qth oscillating term is determined by the nth and n_0th amplitudes of the qth QE eigenfunction C_n^q. A transition from the n_0th to the nth Landau level will occur provided both coefficients C_n^q and $C_{n_0}^{q*}$ in Eq. (16) are large. If we consider the transitions between the quantum separatrices, then the main contribution to the evolution comes from the separatrix QE eigenfunctions as they have their maxima at the various separatrix regions and the diffusion over the quantum separatrices is due to their delocalization. The number of separatrix QE eigenfunctions is very small, but their effect on the diffusion via the separatrices is crucial because localized QE eigenfunctions have minima in the vicinity of the separatrices and do not contribute to this process.

First, let us look at the diffusion over the quantum separatrices in the resonance approximation where the system possesses no chaos. To this end, we place an initial state $C_n(0)=\delta_{n,n_0}$ in the separatrix region and follow the evolution of this state for a sufficiently long time in order to determine the position in Hilbert space of the quantum particle at time $t\to\infty$. The largest characteristic time in the system is $t_{max}=2\pi/\omega_{min}$, where ω_{min} is the minimal distance between the effective QE eigenvalues, i.e., the eigenvalues corresponding to the eigenstates that constitute the initial state and determine the dynamics. As shown above, in our case the effective eigenstates are the separatrix ones. After a time t_{max} the dynamics enters into a quasistationary regime and it is convenient to time average the probability in the region $t\gg t_{max}$ in order to eliminate the influence of fluctuations and exclude transient effects.

The results of this procedure are plotted in Figs. 4(a) and 4(b) for the same h as in Fig. 2 and for two different values of V_0; the initial state, marked with a large arrow, was situated at the Landau level $n_0=20$ in the second cell near the boundary of the first one. From Fig. 4(a) one may note that the time-averaged probability distribution $\langle P_n\rangle$ in the classically inaccessible cells (even in the resonance approximation, where $V_0\to 0$) is comparable to that of the initial (second) cell. It was numerically confirmed that if an initial state $C_{n_0}(0)$ is situated anywhere in the central region of a resonance cell, then only an exponentially small part of a wave packet tunnels to the neighboring cells and a logarithmic scale (in the probability distribution) is necessary in order to recognize the tunneling phenomenon [12]. The second principal point is the observation that the probability distribution in Fig. 4(a) is highest around the boundaries of the quantum resonance cells, always being relatively small in the central regions. Thus anomalously intensive tunneling takes place only between the quantum separatrices and we may refer to this process as ''diffusion via the quantum separatrices.'' This effect is reminiscent of the diffusion of a classical particle within the stochastic web. That idea is supported by the Husimi function of the initially δ-like wave packet after evolution during a rescaled time $\tau=3000$ [see Fig. 5(a)]. This figure reminds us of the web structure in its corresponding classical phase space. However, this effect is of a pure quan-

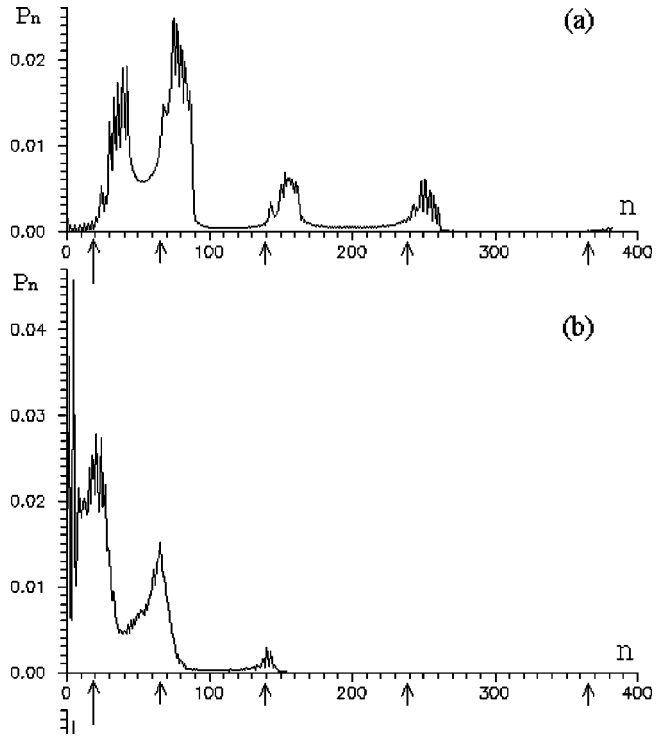

FIG. 4. Time-averaged probability distribution $\langle P_n \rangle$ versus n for $h=0.37$, $N=381$, and (a) $V_0=0.002$ and (b) $V_0=6$. Averaging was performed over 300 times in the region $3000<\tau<6000$ ($\tau=V_0 t$; t is measured in units of the external field period $T=2\pi/\omega$). The separatrix positions are marked with arrows.

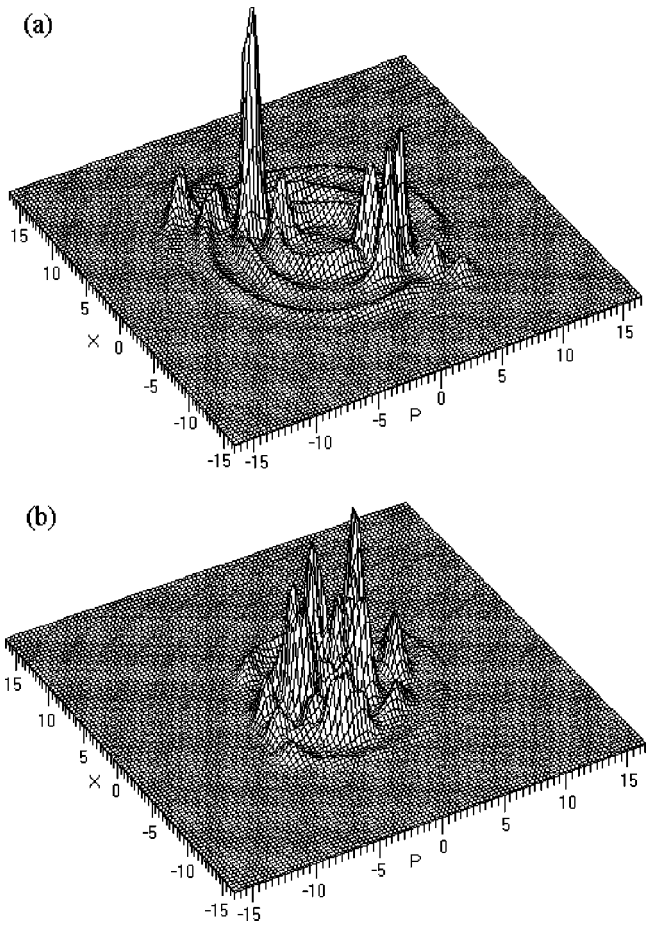

FIG. 5. Husimi functions of the states for the same parameters and initial conditions as in Fig. 4 at (dimensionless) time $\tau=3000$, $C_n(0)=\delta_{n,n_0}$, $n_0=20$, and (a) $V_0=0.002$ and(b) $V_0=6$.

tum nature as the classical particle in the resonance approximation has no possibility of penetrating one cell from another.

The effect of weak chaos on the diffusion over the separatrices is illustrated in Fig. 4(b). Inspection of Figs. 4(a) and 4(b) shows that an increase of the amplitude leads to a decrease of the diffusion rate. This effect of chaos on quantum diffusion is rather unexpected: The increase in the perturbation inhibits tunneling instead of intensifying it. This is a direct consequence of the partial localization of the separatrix QE eigenfunctions of Fig. 2(b) caused by the presence of weak chaos in the vicinity of the separatrix. This quantum weak chaos effect is manifested in the plot of the Husimi function of the wave packet $C_n(0)=\delta_{n,n_0}$ after evolution during the time $\tau=3000$ [see Fig. 5(b)]. Hereinafter the time t is measured in units of T. The third separatrix is not as clearly defined as in Fig. 5(a) or in Fig. 3, being partially destroyed by chaos. The Husimi function looks like the classical density distribution within the stochastic web in phase space (see Fig. 5.7 in Ref. [2]). The fourth and fifth separatrices are absent and the Husimi function appears to be more localized than in the resonance approximation. The structure of the Husimi function within the first two cells is irregular, consistent with the more developed (not weak) chaos in this region.

The phenomenon of localization becomes more evident in Fig. 6, where we show the evolution of the squared dispersion σ^2 as a function of the rescaled time $\tau=V_0 t$. The two chosen values of the perturbation amplitude V_0 correspond, respectively, to the resonance approximation and the regime of weak chaos [the values of h and initial conditions in Fig. 6 are the same as in Figs. 4(a) and 4(b)]. We see from Fig. 6 that the diffusion over the separatrices at $V_0=6$ is suppressed in comparison to the resonance case, consistent with the dynamical picture of Fig. 4. The data shown in Fig. 6 allow us to estimate the effective time of saturation of the probability distribution $\tau_{max}=V_0 t_{max}$. As the wave packet

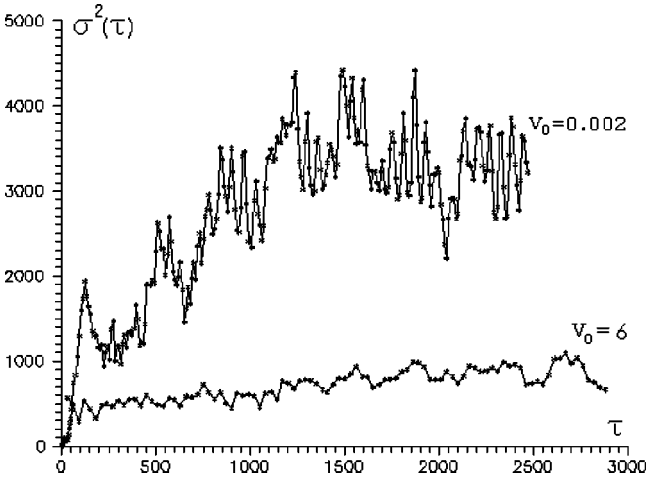

FIG. 6. Dynamics of the squared dispersion $\sigma^2(\tau)$ for the same parameters and initial conditions as in Figs. 4(a) and 4(b) in units of dimensionless time.

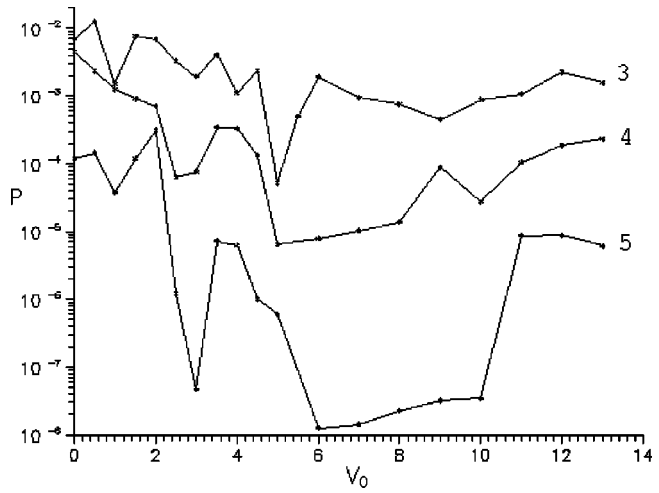

FIG. 7. Diffusion rate P_i of an initially δ-like wave packet, placed at $n_0=20$, from the initial (first) separatrix to the ith one for $i=3,4,5$ as a function of the perturbation amplitude V_0. $h=0.37$ and $N=401$.

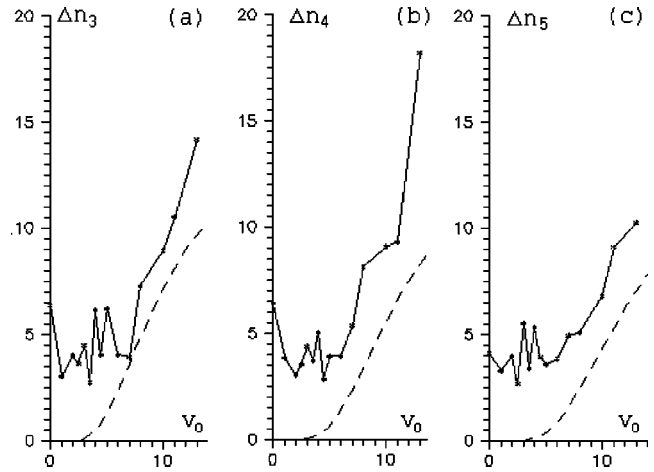

FIG. 8. Widths of the quantum separatrices Δn_i versus the perturbation amplitude V_0 for the same parameters, initial conditions, and separatrices as in Fig. 7.

in Fig. 6 for $V_0=0.002$ spreads over all the separatrices, the effective time in this case is defined by the minimal distance between the separatrix QE eigenvalues; in the presence of weak chaos ($V_0=6$) τ_{max} is mainly determined by the minimal distance between the QE eigenvalues within the initial cell because the probability distribution does not evolve to the other cells. The separatrix QE eigenvalues are situated near the center of the spectrum where the spectrum is dense and the distances between these levels are smallest [11]. Thus a large difference in the values of τ_{max} in the two cases of Fig. 6 arises from the different types of effective eigenstates that determine the dynamics, namely, $\tau_{max}(V_0=0.002) \gg \tau_{max}(V_0=6)$.

We will now show that the diffusion rate can be characterized by two parameters of the probability distribution P_n in the neighborhood of each separatrix *i*. These are the maxima of P_n, denoted by P_i, and its width Δn_i. Plots such as Fig. 4(a) suggest that the distribution P_n in the neighborhood of the separatrix *i*, averaged over time, may be approximated by a Gaussian curve. Then the maxima P_i (width Δn_i) is given by the height (width) of the corresponding Gaussian. Plots of P_i as a function of the perturbation amplitude V_0 give a measure of the diffusion rate. An inspection of Fig. 7 reveals an exponential decrease of the diffusion rate up to the value $V_0' \simeq 6$ (V_0' depends on h). This provides further evidence of the suppression of quantum diffusion over the separatrices due to weak chaos. A further increase of V_0 results in a growth of the diffusion rate, which can be explained by the average increase in the localization length discussed in Sec. III. Such behavior as a function of amplitude corresponds to the classical situation. The minimum in the curve V_0' is the crossover from the quantum to the classical diffusion. The further the boundary of the resonant cell is from the boundary where the initial state was situated, the smaller the minimum is in the corresponding curve because chaos destroys a larger number of delocalized separatrix eigenfunctions that contribute to the diffusion. We speculate that the oscillations of the curves in Fig. 7 arise from the fact that the diffusion over the quantum separatrices is determined by a small number of (separatrix) QE eigenstates and turn out to be very sensitive to changes in the structure of the QE eigenfunctions.

Now consider the plots of the widths Δn_i versus the wave amplitude V_0 shown in Figs. 8(a)–8(c) for the same parameters, initial conditions, and separatrices as in Fig. 7. The data, presented in Fig. 8 have the following interesting features. (i) Consistent with the above considerations [see Eq. (15)], the widths of the quantum separatrices at $V_0 < V_0'$ are approximately the same for all the separatrices and for all values of h (the latter was confirmed by our calculations with other values of h). (ii) On average, the widths Δn_i do not change significantly with V_0 until the amplitude of the perturbation reaches some value V_0', after which the Δn_i begin to grow monotonically. Thus, in the region $V_0 < V_0'$, classical chaos does not affect the width of the quantum separatrices (but does affect the diffusion rate in Fig. 7). (iii) The threshold V_0' in the plot of $\Delta n_i(V_0)$ is the same as the threshold (position of the minimum) in the plot of $P_i(V_0)$ in Fig. 7. At that point the width of the quantum separatrix exceeds the width of the classical stochastic web ΔH_i, which can be approximated by [2]

$$\frac{\Delta H_i}{\hbar\omega_c} = 2^{1/2}\pi^{7/2}\frac{(2hn_i)^{1/2}}{V_0 h^2}\exp\left[\left(-\frac{\pi}{2}\right)^{5/2}\frac{(2hn_i)^{1/2}}{V_0 h}\right], \tag{17}$$

where n_i is the center of the *i*th cell and the quantity hn in the quasiclassical limit becomes the action *I*. The results of our calculations using Eq. (17) are presented in Figs. 8(a)–8(c) with dashed lines. The discrepancy between the quantum and classical curves may presumably be attributed to the approximate character of Eq. (17), which is valid only in the case of an exponentially thin separatrix. Nonetheless, the trend of the quantum curves is qualitatively the same as the classical behavior.

V. CONCLUSION

The numerical data and qualitative analysis presented in this paper allow us to make the following conclusions about the nature of quantum weak chaos. In the quantum resonance

approximation we investigated the resonance structure of Hilbert space and also the new phenomenom of quantum diffusion via the separatrix. We remark that this quantum diffusion has no classical analog because classically, the orbits are confined to resonance cells. In quantum mechanics, this diffusion results from tunneling across the quantum separatrices. An accidental intersection of levels of different cells (associated with the overlap of QE functions) with eigenvalues $E_q \ll V_0$ leads to the formation of delocalized QE eigenfunctions. In other words, the cell structure of the evolution operator matrix (and the Floquet Hamiltonian matrix) gives rise to a long-range coupling between states of different cells. The dynamical manifestation of this effect is an anomalously large diffusion rate between the cells via the quantum separatrices. For sufficiently large values of V_0 the nonresonant terms may be considered as an effective random perturbation that inhibits the long-range interaction, thereby localizing the QE eigenstates.

When the perturbation becomes strong enough diffusion is recovered, but now it is of a completely different nature. Namely, for large values of the perturbation we observe an analog of the classical diffusion within the stochastic web. This is demonstrated by comparing the widths of the classical and quantum separatrices. The structure of the quasienergy eigenstates that explains the diffusion is also different: In the resonance case they have the regular form, which is maintained over several cells of Hilbert space, while at large V_0 such states are destroyed and diffusion takes place because the localization lengths of many QE eigenstates increase on the average.

In this paper the evolution operator propagating the system toward an arbitrary number of periods of the external field is built in the Hamiltonian $\hat{H}_0$ basis. Its eigenstates (QE eigenstates) are explored under the condition of resonance in the regime of weak chaos. In the new phenomenon of diffusion over the quantum separatrices it was found that a small number of delocalized separatrix QE eigenstates play the dominant role. It was shown that weak quantum chaos leads to the localization of the separatrix eigenstates and hence to suppression of quantum diffusion via the separatrices. At large values of perturbation, $V_0 > V_0'$, we have observed a recovery of the diffusion that was associated in the quasiclassical limit with the growth of the classical stochastic web in phase space.

It is necessary to point out that the parameters chosen in our numerical experiments correspond to actual experimental situations. Acoustic cyclotron resonance can be observed in a two-dimensional electron gas in semiconductor heterostructures subject to a transverse magnetic field and in the field of a longitudinal sound wave. In order to observe this phenomenon the electron relaxation time τ_p must be large enough to satisfy the inequality $\omega_c \tau_p \gg 1$. Under this condition and under the condition of cyclotron resonance, one can choose parameters that allow the Fermi level n_F to be placed at the boundary (quantum separatix) between the first and second cells. That is, the argument of the Bessel function $J_1(ka\sqrt{2n_F})$ must coincide with the first zero of the Bessel function J_1. In order to create this situation in an experiment one can choose the following experimental parameters: The sound wave frequency should be of the order of 10 GHz, the magnetic field $H = 2 \times 10^3$ Oe, the effective electron mass $m^* = 0.7 m_e$, and the electron concentration $\mathcal{N} = 10^{11}$ cm^{-2}. These parameters give $h = 0.4$ and $n_0 = n_F = 20$. The value of the parameter V_0 is determined by the deformation div($\mathbf{u}$) $\sim k u_0$, where u_0 is the acoustic wave amplitude. Thus the value $V_0 = 10$ corresponds to the wave deformation $k u_0 \sim 10^{-4}$–10^{-5}. When the proposed parameters are realized in an experiment we predict that quantum chaos will be manifested as, for example, an attenuation of the sound wave.

ACKNOWLEGMENTS

We thank Felix Izrailev for illuminating discussions. This work was performed with the support of INCAS (Grant No. 97-2-15) and the Russian Foundation for Basic Research (Grant No. 98-02-16412). G.A.L.-A. acknowledges partial support from CONACYT (Mexico) under Grant No. 26163-E.

[1] Even though the KAM theorem is not valid for degenerate systems, the phase space structure of KAM theory is present in some cases, e.g., the Hénon-Heiles system. See, for example, A.J. Lichtenberg and M.A. Lieberman, *Regular and Stochastic Motion* (Springer-Verlag, New York, 1983), Sec. 3.2a.

[2] G.M. Zaslavsky, R.Z. Sagdeev, D.A. Usikov, and A.A. Chernikov, *Weak Chaos and Quasiregular Patterns* (Cambridge University Press, Cambridge, 1991); A.A. Chernikov, M.Ya. Natenson, B.A. Petrovichev, R.Z. Sagdeev, and G.M. Zaslavsky, Phys. Lett. A **122**, 39 (1987).

[3] I. Dana and M. Amit, Phys. Rev. E **51**, R2731 (1994).

[4] S. Pekarsky and V. Rom-Kedar, Phys. Lett. A **225**, 274 (1997).

[5] G.P. Berman, V.Uy. Rubaev, and G.M. Zaslavsky, Nonlinearity **4**, 543 (1991).

[6] I. Dana, Phys. Rev. Lett. **73**, 1609 (1994).

[7] G. Casati, B.V. Chirikov, J. Ford, and F.M. Izrailev, Lect. Notes Phys. **93**, 334 (1979).

[8] R. Lima and D. Shepeliansky, Phys. Rev. Lett. **67**, 1377 (1991).

[9] T. Geisel, R. Ketzmerick, and G. Petschel, Phys. Rev. Lett. **67**, 3635 (1991).

[10] I. Dana, Phys. Lett. A **197**, 413 (1995).

[11] V.Ya. Demikhovskii, D.I. Kamenev, and G.A. Luna-Acosta, Phys. Rev. E **52**, 3351 (1995).

[12] V.Ya. Demikhovskii and D.I. Kamenev, Phys. Lett. A **228**, 391 (1997).

[13] F.M. Izrailev, Phys. Rep. **196**, 299 (1990).

[14] G. Casati, I. Guarneri, F.M. Izrailev, and R. Scharf, Phys. Rev. Lett. **64**, 5 (1990)

[15] I.S. Gradshteyn and I.M. Ryzhik, *Table of Integrals, Series and Products* (Academic, New York, 1980).

[16] L.E. Reichl, *The Transition to Chaos* (Springer-Verlag, New York, 1992).

[17] L.E. Reichl and W.A. Lin, Phys. Rev. A **40**, 1055 (1989).

[18] A.J. Lichtenberg and M.A. Lieberman, *Regular and Stochastic Motion* (Springer, New York, 1983), Chap. 2.

[19] M. Kohmoto and Y. Hatsugai, Phys. Rev. B **41**, 9527 (1990).

[20] K. Husimi, Proc. Phys. Math. Soc. Jpn. **22**, 264 (1940).